Improved Damping Control of Grid-forming Inverter Using DC Dynamics

Chen, Meng; Zhou, Dao; Blaabjerg, Frede

Published in:
Proceedings of the 2023 IEEE 17th International Conference on Compatibility, Power Electronics and Power Engineering (CPE-POWERENG)

DOI (link to publication from Publisher):
10.1109/CPE-POWERENG58103.2023.10227457

Publication date:
2023

Document Version
Accepted author manuscript, peer reviewed version

Improved Damping Control of Grid-forming Inverter Using DC Dynamics

Meng Chen, Dao Zhou, and Frede Blaabjerg
AAU Energy
Aalborg University
Aalborg, Denmark
mche@energy.aau.dk, zda@energy.aau.dk, fbl@et.aau.dk

***Abstract*—The DC side of the grid-forming inverter is usually simplified as an ideal source when considering the AC dynamics. However, the DC dynamics actually contain useful information of the AC side. This paper proposes an improved damping control for the grid-forming inverter using the DC dynamics. The error of the DC voltage is introduced into the active power loop through a proportional controller. As a result, an extra freedom in addition to the virtual inertia can be adjusted. A small-signal analysis is carried out in detail to study the impact of the DC dynamics. Compared with other damping methods, the proposed method can simultaneously improve the performance of not only the AC side but also the DC side without increasing the order of the system The simulation results verify the effectiveness of the proposed method.**

***Index Terms*—DC dynamics, grid-forming inverter, AC dynamics, loop coupling, damping control**

I. Introduction

To cope with the challenges of the air pollution and the energy shortage, more and more renewable energy sources (RESs) are connected into the AC power system, most of which have the inverters as interfaces [1]. Conventionally, the inverters are required to output the references though a vector control without providing other auxiliary services, which synchronizes to the grid via a phase-locked loop (PLL). Such inverter is call grid-following (GFL) inverter [2].

However, the lack of frequency and voltage regulation ability of the grid-following inverters limits a further increasing of the penetration of the RESs. The power system with a large penetration of GFL inverters may have small stability margins or even suffer instability from various disturbances [3]. Therefore, the grid-forming (GFM) inverter are drawn much attention lately, where its frequency and voltage can be kept stable without relying on an external power grid [4].

Although various GFM controls have been proposed, one of the basic characteristics of them is the droop characteristics [5]. It can been proved that the droop coefficients provide the damping equivalently to improve the stability of the system [6]. Nevertheless, the basic droop control cannot provide inertia, which is an important index to the power system. A small inertia leads to a large rate-of-change-of-frequency (RoCoF) and a low frequency nadir, which are harmful to the frequency stability and frequency-sensitive loads [7]. To keep the equivalent inertia while increasing the penetration of RESs, the virtual inertia is combined with the droop characteristics to form the virtual synchronous generator (VSG) control [8].

The VSG can provides a large inertia at the expenses of small power oscillations [9]. In this context, the damping control is one of the most important topics to the VSG-based GFM inverter, among which changing the droop coefficient is the simplest method. However, it is not recommended due to the fact that the droop coefficient is usually determined by the expected droop characteristics rather than the damping [10]. Therefore, an extra freedom should be added to regulate the damping. Based on this principle, a PLL-based damping strategy is popular [11]. Moreover, the high-frequency component of the VSG frequency can be used as well [12]. In [13], a damping strategy is designed consisting of the terms of acceleration control and active power suppression. In [10], it is the virtual flux in the reactive power loop which is used to construct the damping in the active power loop. There are other damping methods as well, which have been verified as useful [14]. Nonetheless, all the above methods increase the order and complexity of the system due to the use of low-pass filter, high-pass filter, PLL, etc.

In addition, in the aforementioned methods, the DC side of the GFM inverter is assumed to be an ideal source. In actual, the DC dynamics are coupled with the AC dynamics due to the power balance. In [15], the $\mathcal{H}_\infty$ optimization is used to design a multi-input multi-output GFM inverter, which has shown that the DC dynamics may be beneficial to the performance of the system, although its detailed influence is not clear.

In this paper, we propose to improve the damping of the GFM inverter, where the following advantages and contributions can be achieved compared with the existing methods

1) Only a simple proportional controller is required without increasing the order and complexity of the whole system.
2) The influence of the DC dynamics are studied in detail through a small-signal analysis.
3) Both the AC and DC sides of the GFM inverter can be improved.

The remainder of paper is organized as follows. The preliminary of the GFM inverter is briefly introduced in Section II. In Section III, the proposed damping control and a detailed small-

This work was supported by the Reliable Power Electronic-Based Power System (REPEPS) project at the Department of Energy Technology, Aalborg University as part of the Villum Investigator Program funded by the Villum Foundation.

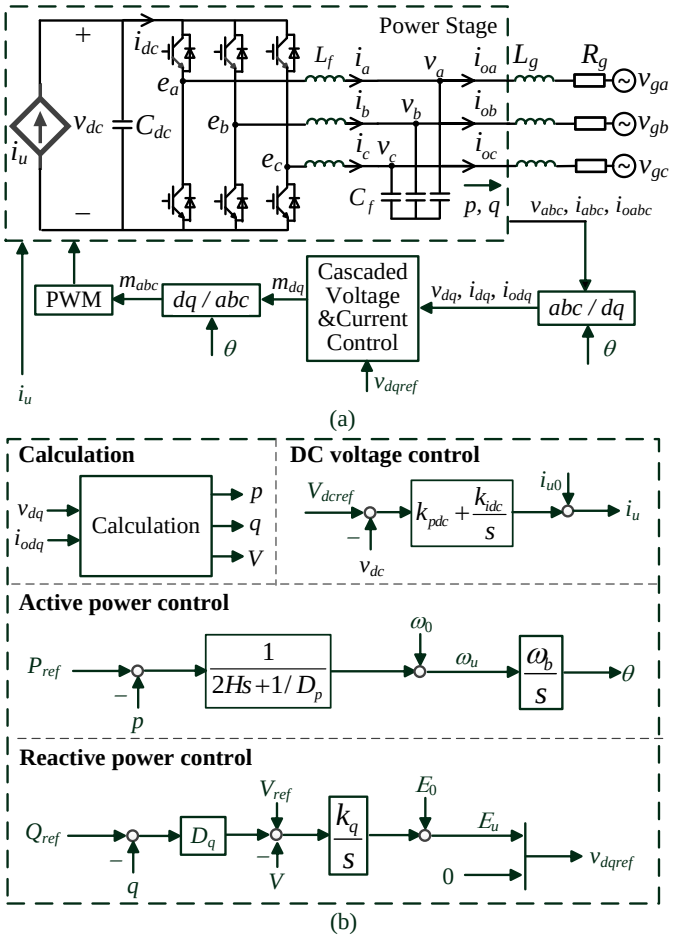

Fig. 1. General configuration of grid-forming converters. (a) Topology with inner loops. (b) Outer power loops and DC voltage loop.

signal analysis are given. In Section IV, simulation results are shown, and finally, conclusions are given in Section V.

II. Preliminary of VSG-Based Grid-Forming Converter

Fig. 1 shows the general configuration of a conventional VSG-based grid-forming power converter. The power stage consists of a typical three-phase inverter as well as an LC filter, where L_f and C_f are the inductor and capacitor of the filter. To consider the DC voltage dynamics, the DC source is represented by a controlled current source i_u paralleled with a DC capacitor C_{dc}. As shown in Fig. 1(a), a cascaded voltage and current control loop is usually used as the inner loop to regulate the inductor current and capacitor voltage of the filter [1]. Therefore, the outer loops are supposed to provide the DC current signal i_u, the voltage references v_{dqref}, and the angle for tranformation θ.

As shown in Fig. 1(b), the outer control of the VSG includes a DC voltage control loop, an active power control loop, and a reactive power control loop. Mostly, the DC voltage control uses a simple PI controller, where the state-space representation can be expressed as

$$\dot{\zeta} = V_{dcref} - v_{dc} \tag{1}$$

$$i_u = k_{idc}\zeta + k_{pdc}(V_{dcref} - v_{dc}) + i_{u0} \tag{2}$$

where ζ is the state variable of the DC voltage control, V_{dcref} and v_{dc} are the reference and actual values of the DC voltage, respectively, k_{pdc} and k_{idc} are the parameters of the PI controller, and i_{u0} is the set-point value of i_u.

The active power control of the VSG emulates the swing equation, which can be expressed as [8]

$$2H\dot{\omega}_u = \frac{1}{D_p}(\omega_0 - \omega_u) + P_{ref} - p \tag{3}$$

$$\dot{\theta} = \omega_b \omega_u \tag{4}$$

where H is the virtual inertia constant, ω_u and ω_0 is the virtual angle frequency and its set-point value, P_{ref} and p are the reference and actual values of the active power, D_p is the droop coefficient of the active power control, and ω_b is the base value of the angle frequency.

The reactive power control of the VSG is based on the droop characteristics as well, where the dynamics can be expressed as

$$\dot{E}_u = k_q(V_{ref} - V) + k_q D_q(Q_{ref} - q) \tag{5}$$

where E_u is the internal voltage of the VSG and is used as v_{dref} as shown in Fig. 1, V_{ref} and V are the reference and actual values of the magnitude of the capacitor voltage, Q_{ref} and q are the reference and actual values of the reactive power, k_q is the interal gain, D_q is the droop coefficient of the reactive power control.

III. Proposed DC Voltage Control Strategy

A. Problem and proposed control structure

Considering an inductive grid, due to the high bandwidths of the cascaded voltage and current loops and the quick dynamics of the line, the active power p can be expressed as

$$p = \frac{VV_g}{X_g} sin\delta \tag{6}$$

where V_g is the magnitude of the grid voltage, X_g is the synchronous reactance of the line, and δ is the angle difference between the VSG and grid reference frames and can be calculated by

$$\dot{\delta} = \omega_b \omega_u - \omega_b \omega_g \tag{7}$$

where ω_g is the grid frequency.

Moreover, if neglecting the power loss of the power stage of the GFM converter, according to Fig. 1(a), the DC power can be estimated using the output active power p. Therefore, the dynamics of the DC capacitor can be expressed as

$$\dot{v}_{dc} = \frac{\omega_b}{C_{dc}} i_u - \frac{\omega_b p}{C_{dc} v_{dc}} \tag{8}$$

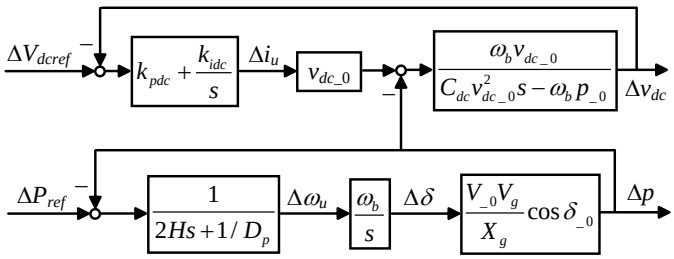

Fig. 2. Small-signal block diagram of active power balance of conventional GFM converter.

The nonlinear model dominating the active power balance of the VSG consists of (1)-(3) and (6)-(8). Thereafter, the corresponding small-signal model can be derived as

$$\Delta\dot{\zeta} = \Delta V_{dcref} - \Delta v_{dc} \tag{9}$$

$$\Delta i_u = k_{idc}\Delta\zeta + k_{pdc}(\Delta V_{dcref} - \Delta v_{dc}) \tag{10}$$

$$\Delta\dot{\omega}_u = -\frac{1}{2HD_p}\Delta\omega_u - \frac{1}{2H}\Delta p + \frac{1}{2H}\Delta P_{ref} \tag{11}$$

$$\Delta p = \frac{V_{\_0}V_g}{X_g}cos\delta_{\_0}\Delta\delta \tag{12}$$

$$\Delta\dot{\delta} = \omega_b\Delta\omega_u \tag{13}$$

$$\Delta\dot{v}_{dc} = \frac{\omega_b}{C_{dc}}\Delta i_u - \frac{\omega_b}{C_{dc}v_{dc\_0}}\Delta p + \frac{\omega_b p_{\_0}}{C_{dc}v_{dc\_0}^2}\Delta v_{dc} \tag{14}$$

where "Δ" denotes the small-signal variable the subscript "$\_0$" denotes the used operating point to linearize the system. The small-signal block diagram is shown in Fig. 2 and the state equation of the DC voltage control and active power control is derived as

$$\Delta\dot{\boldsymbol{x}} = \boldsymbol{A}_{VSG}\boldsymbol{\Delta x} + \boldsymbol{B}_{VSG}\boldsymbol{\Delta u} \tag{15}$$

where

$$\boldsymbol{x} = \begin{bmatrix}\omega_u & \delta & v_{dc} & \zeta\end{bmatrix}^T,\ \boldsymbol{u} = \begin{bmatrix}P_{ref} & V_{dcref}\end{bmatrix}^T \tag{16}$$

$$\boldsymbol{A}_{VSG} = \begin{bmatrix} -\frac{1}{2HD_p} & -\frac{V_{\_0}V_g cos\delta_{\_0}}{2HX_g} & 0 & 0 \\ \omega_b & 0 & 0 & 0 \\ 0 & -\frac{\omega_b V_{\_0}V_g cos\delta_{\_0}}{C_{dc}v_{dc\_0}X_g} & \frac{\omega_b(p_{\_0}-k_{pdc}v_{dc\_0}^2)}{C_{dc}v_{dc\_0}^2} & \frac{\omega_b k_{idc}}{C_{dc}} \\ 0 & 0 & -1 & 0 \end{bmatrix} \tag{17}$$

$$\boldsymbol{B}_{VSG} = \begin{bmatrix} \frac{1}{2H} & 0 & 0 & 0 \\ 0 & 0 & \frac{\omega_b k_{pdc}}{C_{dc}} & 1 \end{bmatrix}^T \tag{18}$$

The eigenvalues of the upper 4th-order model can be tuned by only three parameters, i.e., H, k_{pdc}, and k_{idc}. Therefore, at least an extra freedom is expected to be introduced.

It is noticed from Fig. 2 that the dynamics of Δv_{dc} is influenced by the AC variables, i.e., Δp, which implies that the DC dynamics are coupled with the AC dynamics. In most of the conventional GFM control methods, this coupling is neglected as the DC side is represented by an ideal source. Donating

$$G_{\omega p}(s) = -\frac{1}{2Hs+1/D_p} \tag{19}$$

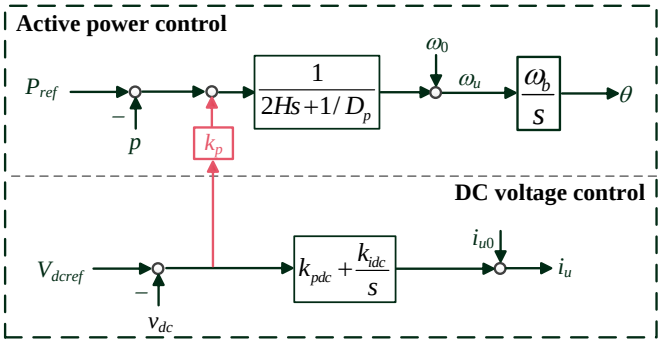

Fig. 3. Proposed novel control structure of GFM converter.

$$G_{DCp}(s) = -\frac{\omega_b v_{dc\_0}s}{C_{dc}v_{dc\_0}^2 s^2 + \omega_b(v_{dc\_0}^2 k_{pdc} - p_{\_0})s + \omega_b v_{dc\_0}^2 k_{idc}} \tag{20}$$

there are, from Fig. 2, that

$$\frac{\Delta\omega_u}{\Delta p} = G_{\omega p}(s),\ \frac{\Delta v_{dc}}{\Delta p} = G_{DCp}(s) \tag{21}$$

where the following equation can be derived

$$\frac{\Delta v_{dc}}{\Delta\omega_u} = \frac{G_{DCp}(s)}{G_{\omega p}(s)} \tag{22}$$

The upper equation present the relationship between Δv_{dc} and $\Delta\omega_u$, which implies that Δv_{dc} may provide a similar damping function with $\Delta\omega_u$. According to the aforementioned analysis, this paper tries to improve the dynamics of the GFM converter taking advantages of the coupling between the AC and DC dynamics. To do so, a new control structure is proposed as shown in Fig. 3, where an additional signal, i.e., the DC voltage error, is introduced into the active power control from the DC voltage control. As a result, the new mathematical expression of the active power control can be expressed as

$$2H\dot{\omega}_u = \frac{1}{D_p}(\omega_0 - \omega_u) + P_{ref} - p + k_p(V_{dcref} - v_{dc}) \tag{23}$$

where k_p is a control gain. It should be mentioned that, in the steady-state, $v_{dc} = V_{dcref}$ is guaranteed by the DC voltage control. Therefore, the proposed method does not influence the steady-state droop characteristics. Meanwhile, no other additional filter is needed as well, which makes the new structure simple without increasing the order of the system.

B. Small-Signal Analysis

Linearizing (24) yields

$$\Delta\dot{\omega}_u = -\frac{1}{2HD_p}\omega_u - \frac{1}{2H}\Delta p - \frac{k_p}{2H}\Delta v_{dc} + \frac{1}{2H}\Delta P_{ref} + \frac{k_p}{2H}\Delta V_{dcref} \tag{24}$$

which combining with (9), (10),(12)-(14) construct the new small-signal model with the proposed method. Accordingly, the updated small-signal block diagram of the active power

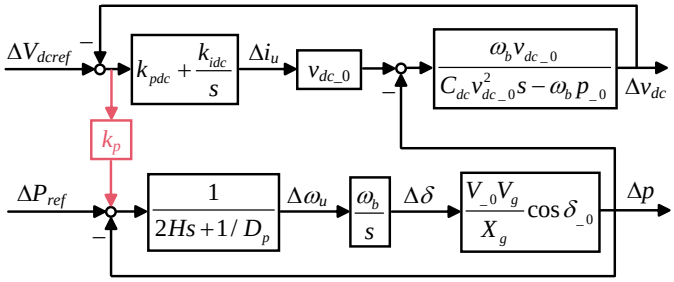

Fig. 4. Small-signal block diagram of active power balance of GFM converter with proposed method.

balance of the GFM converter is shown in Fig. 4. Therefore, the following state equation can be derived:

$$\Delta\dot{\boldsymbol{x}} = \boldsymbol{A}_{new}\boldsymbol{\Delta x} + \boldsymbol{B}_{new}\boldsymbol{\Delta u} \tag{25}$$

where

$$\boldsymbol{A}_{new} = \begin{bmatrix} -\frac{1}{2HD_p} & -\frac{V_{\_0}V_g cos\delta_{\_0}}{2HX_g} & -\frac{k_p}{2H} & 0 \\ \omega_b & 0 & 0 & 0 \\ 0 & -\frac{\omega_b V_{\_0}V_g cos\delta_{\_0}}{C_{dc}v_{dc\_0}X_g} & \frac{\omega_b(p_{\_0}-k_{pdc}v_{dc\_0}^2)}{C_{dc}v_{dc\_0}^2} & \frac{\omega_b k_{idc}}{C_{dc}} \\ 0 & 0 & -1 & 0 \end{bmatrix} \tag{26}$$

$$\boldsymbol{B}_{VSG} = \begin{bmatrix} \frac{1}{2H} & 0 & 0 & 0 \\ \frac{k_p}{2H} & 0 & \frac{\omega_b k_{pdc}}{C_{dc}} & 1 \end{bmatrix}^T \tag{27}$$

By comparing (26) with (17), it is observed that k_p is added and can be used to tune the locations of the eigenvalues. Considering the steady-state operating point and parameters in Table I, Fig. 5 shows the loci of the eigenvalues when k_p changes from -20 to 20 with different H. As observed, there is a negative real eigenvalue, which is always far away from the imaginary axis and is not affected by H and k_p. Both H and k_p will influence the other three eigenvalues. As H increases, all the three affected eigenvalues move towards the imaginary axis in the left-hand s-plane. Therefore, although a larger H can decrease the oscillatory frequency, i.e, RoCoF, the stability and settle time may be highly deteriorated. That is the reason why only H is not adequate to tune the dynamics in the conventional VSG. In comparison, a large k_p make the affected negative real eigenvalue move towards left. Meanwhile, it is also observed that k_p will influence both the damping ratio and oscillatory frequency. Thus, with the help of k_p, a small oscillation can be achieved while still keeping a small RoCoF.

IV. Simulation Results

In this section, the effectiveness of the proposed method is verified via time-domain simulations in Matlab/Simulink. The system is the same as Fig. 1, where the parameters are listed in Table II. The disturbances are added as follows:

- $t = 5$ s, P_{ref} increases from 0.5 p.u. to 1 p.u.
- $t = 8$ s, V_{dcref} increase from 1 p.u. to 1.01 p.u.

Fig. 6 presents the simulation results of the conventional VSG with different inertia constant H. As expected, a larger

TABLE I
Steady-State Operating Point and Parameters for Small-Signal Analysis

Symbol	Value	Symble	Value
$V_{\_0}$	1 p.u.	$\delta_{\_0}$	0.0435 rad
v_{dc_0}	1 p.u.	$p_{\_0}$	0.5 p.u.
V_g	1 p.u.	X_g	0.087 p.u.
ω_b	100π	C_{dc}	15.4 p.u.
k_{idc}	150	D_p	0.01 p.u.
k_{pdc}	40		

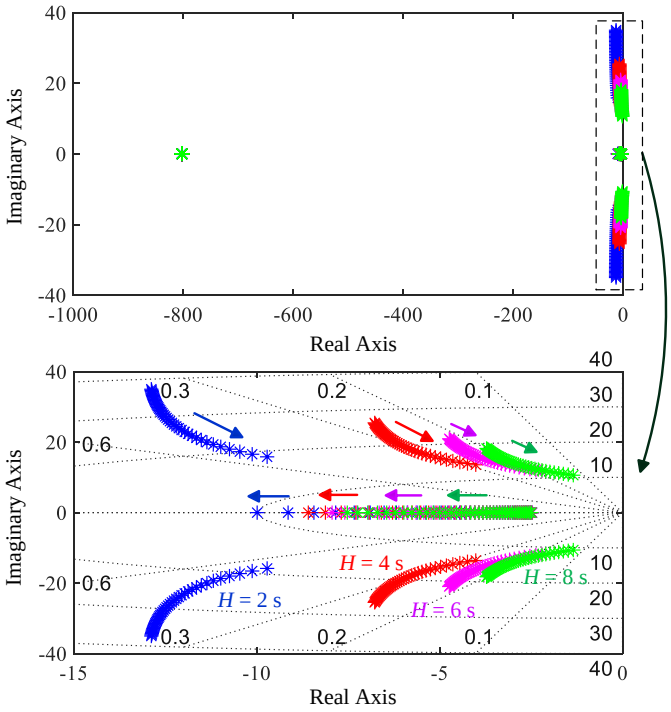

Fig. 5. Loci of the eigenvalues when k_p changes from -20 to 20 with different H.

H decreases the oscillatory frequencies of the output power p and frequency ω_u, which implies, especially, a smaller RoCoF. Nevertheless, there always are large oscillations to be observed. Moreover, it is worth highlighting that, from Fig. 6(c), the disturbance in the AC side will also lead to oscillations in the DC dynamics, where the smaller H is the more quickly v_{dc} decreases. Meanwhile, dynamic with the smallest $H = 2$ s has the lowest transient DC voltage. It is also noticed that the DC disturbance will not influence the AC dynamics in the conventional VSG.

Now considering the proposed GFM control, Fig. 7 presents the simulation results with different k_p while H is kept as 8 s to have a small RoCoF. As observed, k_p does not change the response speeds at the beginning of the disturbance of various variables, e.g., the RoCoF. However, a negative k_p can decrease the overshoot of the active power and the maximum

TABLE II
PARAMETERS OF STUDIED SYSTEM

Symbol	Description	Value
f_n	Nominal frequency	100π rad/s
S_n	Nominal power	5 kW
V_n	Nominal line-to-line RMS voltage	380 V
V_{dcn}	Nominal DC voltage	700 V
ω_g	Grid frequency	100π rad/s (1 p.u.)
V_g	Line-to-line RMS grid voltage	380 V (1 p.u.)
L_g	Line inductor	8 mH (0.087 p.u.)
R_g	Line resistor	0.24 Ω (0.008 p.u.)
C_f	Filter capacitor	5 μF (0.0454 p.u.)
L_f	Filter inductor	3 mH (0.0326 p.u.)
C_{dc}	DC capacitor	500 μF (15.4 p.u.)
D_p	Droop coefficient of P-f regulation	0.01 p.u.
D_q	Droop coefficient of Q-V regulation	0.05 p.u.
ω_{set}	Frequency reference	1 p.u.
P_{set}	Active power reference	0.5 p.u.
Q_{set}	Reactive power reference	0 p.u.
V_{set}	Voltage magnitude reference	1 p.u.
k_q	Gain of reactive power control	10
k_{pdc}	Proporional gain of DC control	40
k_{idc}	Integral gain of DC control	150

frequency deviation, and improve the DC dynamics responding to a AC disturbance. It is also observed that, as the DC dynamic is introduced in the AC side, the AC variables will be influenced more obviously when there is a DC disturbance. Nevertheless, the impact is quite small.

V. CONCLUSION

This paper proposes a new grid-forming control strategy with an enhanced damping ability. The additional damping is achieved via dynamics coupling between the AC and DC sides. A detailed small-signal analysis is carried out. The effectiveness of the proposed method is verified by time-domain simulations. The results show that the proposed method can decrease the oscillations in the DC and AC sides while keeping a small RoCoF using only simple proportional controller without increasing the complexity of the system.

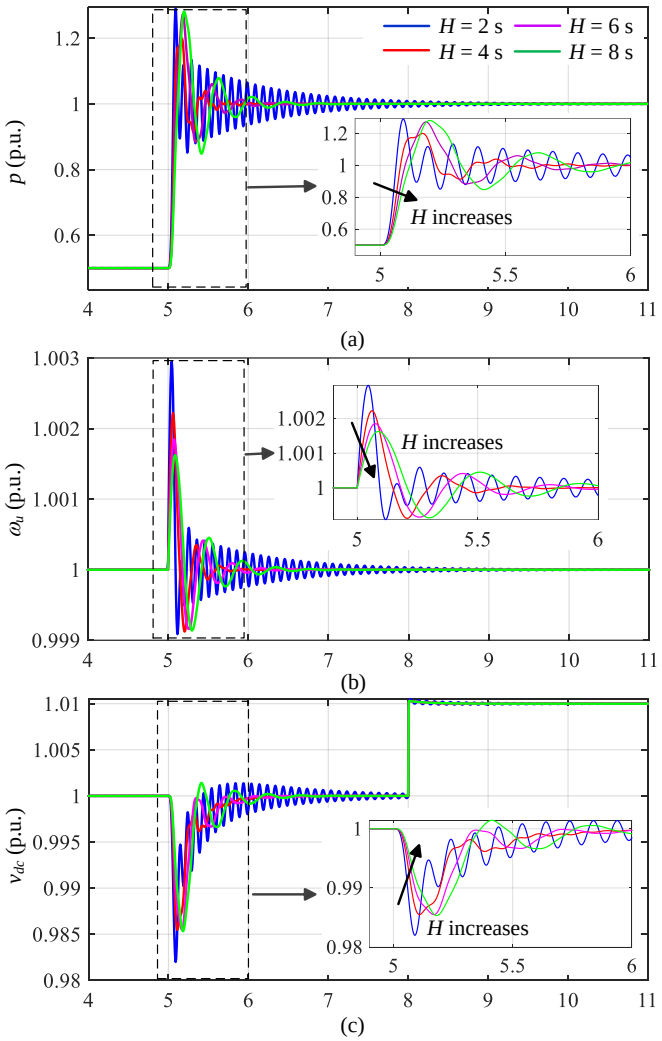

Fig. 6. Simulation results of conventional VSG with different H. (a) Output active power. (b) Frequency. (c) DC voltage.

REFERENCES

[1] H. Zhang, W. Xiang, W. Lin, and J. Wen, "Grid forming converters in renewable energy sources dominated power grid: Control strategy, stability, application, and challenges," *J. Mod. Power Syst. Clean Energy*, vol. 9, no. 6, pp. 1239–1256, Nov. 2021.

[2] J. Song, M. Cheah-Mane, E. Prieto-Araujo, and O. Gomis-Bellmunt, "Short-circuit analysis of AC distribution systems dominated by voltage source converters considering converter limitations," *IEEE Trans. Smart Grid*, vol. 13, no. 5, pp. 3867–3878, Sep. 2022.

[3] O. Stanojev, U. Markovic, P. Aristidou, and G. Hug, "Improving stability of low-inertia systems using virtual induction machine synchronization for grid-following converters," *IEEE Trans. Power Syst.*, pp. 1–14, 2022.

[4] A. Tayyebi, A. Anta, and F. Dörfler, "Grid-forming hybrid angle control and almost global stability of the DC-AC power converter," *IEEE Trans. Autom. Control*, pp. 1–16, 2022.

[5] N. Mohammed and M. Ciobotaru, "Adaptive power control strategy for smart droop-based grid-connected inverters," *IEEE Trans. Smart Grid*, vol. 13, no. 3, pp. 2075–2085, May 2022.

[6] Z. Wang, H. Yi, F. Zhuo, J. Wu, and C. Zhu, "Analysis of parameter influence on transient active power circulation among different generation units in microgrid," *IEEE Trans. Ind. Electron.*, vol. 68, no. 1, pp. 248–257, Jan. 2021.

[7] C. Li, Y. Cao, Y. Yang, J. Xu, M. Wu, W. Zhang, and T. Dragicevic, "New framework of RoCoF-FD for wideband stability evaluation in renewable energy generators with virtual impedance control," *IEEE Trans. Smart Grid*, vol. 13, no. 5, pp. 3570–3581, Sep. 2022.

[8] M. Chen, D. Zhou, and F. Blaabjerg, "Enhanced transient angle stability control of grid-forming converter based on virtual synchronous generator," *IEEE Trans. Ind. Electron.*, vol. 69, no. 9, pp. 9133–9144, Sep. 2022.

[9] M. Chen, D. Zhou, C. Wu, and F. Blaabjerg, "Characteristics of parallel inverters applying virtual synchronous generator control," *IEEE Trans. Smart Grid*, vol. 12, no. 6, pp. 4690–4701, Nov. 2021.

[10] S. Dong and Y. C. Chen, "A method to directly compute synchronverter parameters for desired dynamic response," *IEEE Trans. Energy Convers.*, vol. 33, no. 2, pp. 814–825, Jun. 2018.

[11] M. N. Ambia, K. Meng, W. Xiao, A. Al-Durra, and Z. Y. Dong, "Interactive grid synchronization-based virtual synchronous generator control scheme on weak grid integration," *IEEE Trans. Smart Grid*, vol. 13, no. 5, pp. 4057–4071, Sep. 2022.

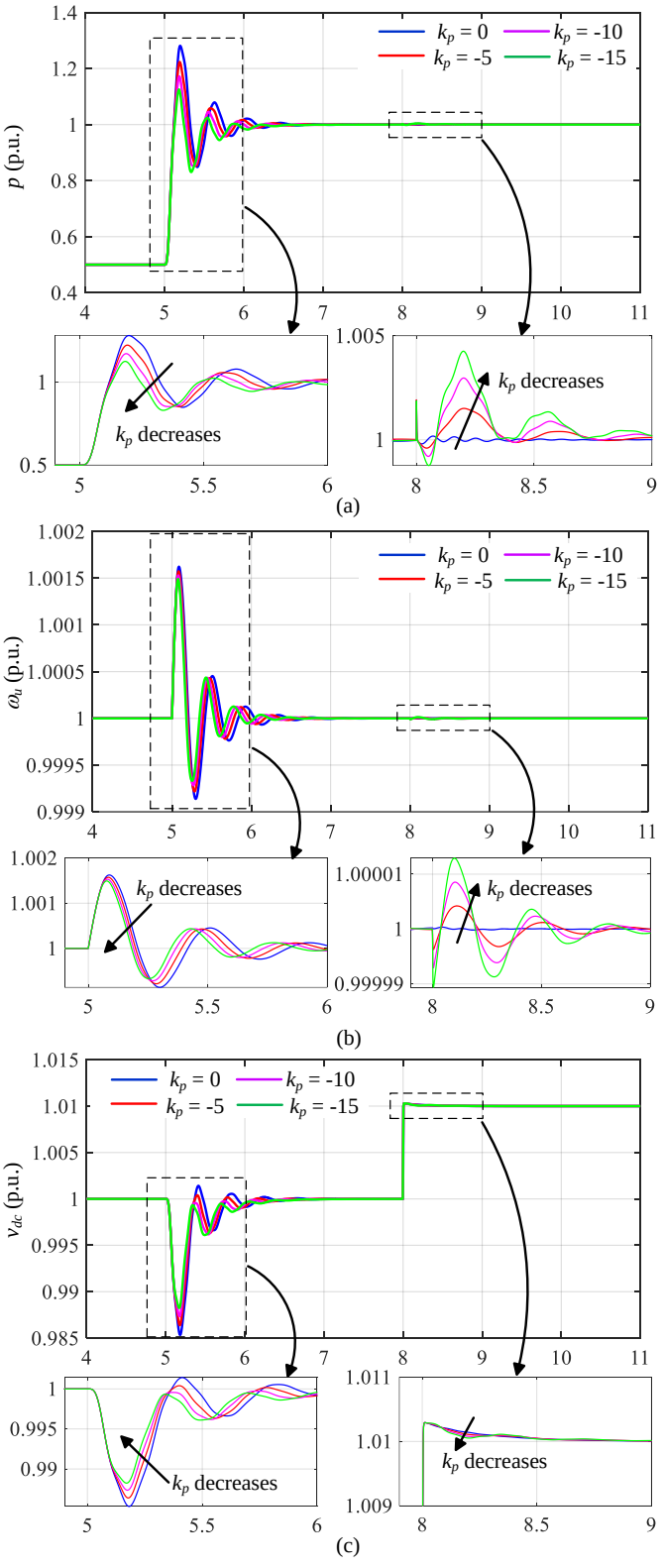

Fig. 7. Simulation results of proposed GFM control with different k_p. (a) Output active power. (b) Frequency. (c) DC voltage.

[12] Z. Shuai, W. Huang, Z. J. Shen, A. Luo, and Z. Tian, "Active power oscillation and suppression techniques between two parallel synchronverters during load fluctuations," *IEEE Trans. Power Electron.*, vol. 35, no. 4, pp. 4127–4142, Apr. 2020.

[13] M. Chen, D. Zhou, and F. Blaabjerg, "Active power oscillation damping based on acceleration control in paralleled virtual synchronous generators system," *IEEE Trans. Power Electron.*, vol. 36, no. 8, pp. 9501–9510, Aug. 2021.

[14] J. Liu, Y. Miura, H. Bevrani, and T. Ise, "A unified modeling method of virtual synchronous generator for multi-operation-mode analyses," *IEEE J. Emerg. Sel. Top. Power Electron.*, vol. 9, no. 2, pp. 2394–2409, Apr. 2021.

[15] M. Chen, D. Zhou, A. Tayyebi, E. Prieto-Araujo, F. Dörfler, and F. Blaabjerg, "Generalized multivariable grid-forming control design for power converters," *IEEE Trans. Smart Grid*, vol. 13, no. 4, pp. 2873–2885, Jul. 2022.